

See discussions, stats, and author profiles for this publication at: <https://www.researchgate.net/publication/260873187>

# Enzyme Immobilization on Si lane-Modified Surface through Short Linkers: Fate of Interfacial Phases and Impact on Catalytic Activity

ARTICLE in LANGMUIR · MARCH 2014

Impact Factor: 4.46 · DOI: 10.1021/la404935q · Source: PubMed

---

CITATIONS

5

READS

36

---

## 6 AUTHORS, INCLUDING:



Aissaoui Nesrine

Chalmers University of Technology

6 PUBLICATIONS 80 CITATIONS

[SEE PROFILE](#)



Latifa Bergaoui

University of Carthage

23 PUBLICATIONS 370 CITATIONS

[SEE PROFILE](#)



Jean-François Lambert

Pierre and Marie Curie University - Paris 6

151 PUBLICATIONS 2,663 CITATIONS

[SEE PROFILE](#)



Jessem Landoulsi

Pierre and Marie Curie University - Paris 6

52 PUBLICATIONS 521 CITATIONS

[SEE PROFILE](#)

## Enzyme Immobilization on Silane-Modified Surface through Short Linkers: Fate of Interfacial Phases and Impact on Catalytic Activity

Nesrine Aissaoui,<sup>†,‡,§</sup> Latifa Bergaoui,<sup>§,||</sup> Souhir Boujday,<sup>†,‡</sup> Jean-François Lambert,<sup>†,‡</sup> Christophe Méthivier,<sup>†,‡</sup> and Jessem Landoulsi\*,<sup>†,‡</sup>

<sup>†</sup>Sorbonne Universités, UPMC Univ Paris 06, F-75005, Paris, France

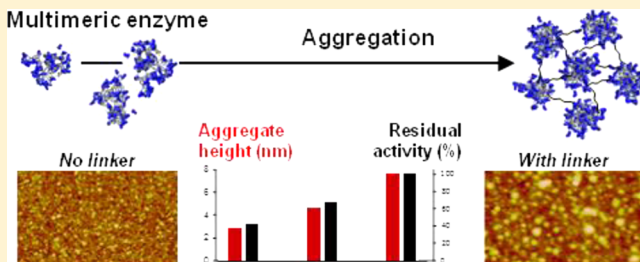
<sup>‡</sup>CNRS, UMR 7197, Laboratoire de Réactivité de Surface, F-75005, Paris, France

<sup>§</sup>Department of Biological and Chemical Engineering, National Institute of Applied Sciences and Technology, INSAT, Centre Urbain Nord BP 676 - 1080 Tunis cedex, Tunisia

<sup>||</sup>Laboratory of Chemistry of Materials and Catalysis, Faculty of Sciences of Tunis, Tunis 2092, Tunisia

### Supporting Information

**ABSTRACT:** We investigated the mechanism of enzyme immobilization on silanized surfaces through coupling agents (cross-linkers) in order to understand the role of these molecules on interfacial processes and their effect on catalytic activity. To this end, we used a model multimeric enzyme (G6PDH) and several cross-linking molecules with different chemical properties, including the nature of the end-group (-NCO, -NCS, -CHO), the connecting chain (aliphatic vs aromatic), and geometrical constraints (meta vs para-disubstituted aromatics). There did not seem to be radical differences in the mechanism of enzyme adsorption according to the linker used as judged from QCM-D, except that in the case of DIC (1,4-phenylene diisocyanate) the adsorption occurred more rapidly. In contrast, the nature of the cross-linker exerted a strong influence on the amount of enzyme immobilized as estimated from XPS, and more unexpectedly on the stability of the underlying silane layer. DIC, PDC (1,4-phenylene diisothiocyanate), or GA (glutaraldehyde) allowed successful enzyme immobilization. When the geometry of the linker was changed from 1,4-phenylene diisothiocyanate to 1,3-phenylene diisothiocyanate (MDC), the silane layer was subjected to degradation, upon enzyme adsorption, and the amount of immobilized molecules was significantly lowered. TE (terephthalaldehyde) and direct enzyme deposition without cross-linker were similar to MDC. The organization of immobilized enzymes also depended on the immobilization procedure, as different degrees of aggregation were observed by AFM. A correlation between the size of the aggregates and the catalytic properties of the enzyme was established, suggesting that aggregation may enhance the thermostability of the multimeric enzyme, probably through a compaction of the 3D structure.



## 1. INTRODUCTION

Enzyme immobilization on solid surfaces is a relevant procedure to preserve catalytic activity and is particularly important in a wide range of biotechnology applications such as anti-biofouling,<sup>1</sup> biochip and biosensors development,<sup>2</sup> and food industries.<sup>3</sup> To achieve enzyme immobilization, the surface of the support material is first chemically modified with the aim of controlling its later interactions with enzyme molecules. Enzyme–solid surface interaction mechanisms may involve a variety of dynamic interfacial processes that are strongly influenced by intrinsic properties of the protein (3-D structure, molecular weight, charge distribution, etc.), surface properties, and physicochemical parameters of the system (temperature, pH, and ion strength of the enzyme solution, etc.). In many situations, the enzyme–surface interactions involve noncovalent links (e.g., hydrophobic interactions, hydrogen bonding, etc.), considered as weak interactions, often preserving the conformation of the molecule, at the

expense of some instability of the immobilization (non-covalently immobilized enzymes may be leached away).<sup>4</sup> In contrast, the immobilization of enzymes through covalent linking may provide a stable attachment that limits desorption and retains the enzyme activity, sometimes even under drastic operational conditions, where free enzymes are generally deactivated.

On oxidized surfaces, enzymes are usually immobilized via an anchoring layer of silanes bearing reactive moieties such as amine functions,<sup>5–7</sup> where covalent attachment (grafting) can be achieved through the use of coupling agents (cross-linkers). The most commonly used cross-linkers carry two similar groups,<sup>8,9</sup> which are able to form a specific covalent bond with the surface at one end and another covalent bond with the

**Received:** May 29, 2013

**Revised:** March 12, 2014

**Published:** March 17, 2014



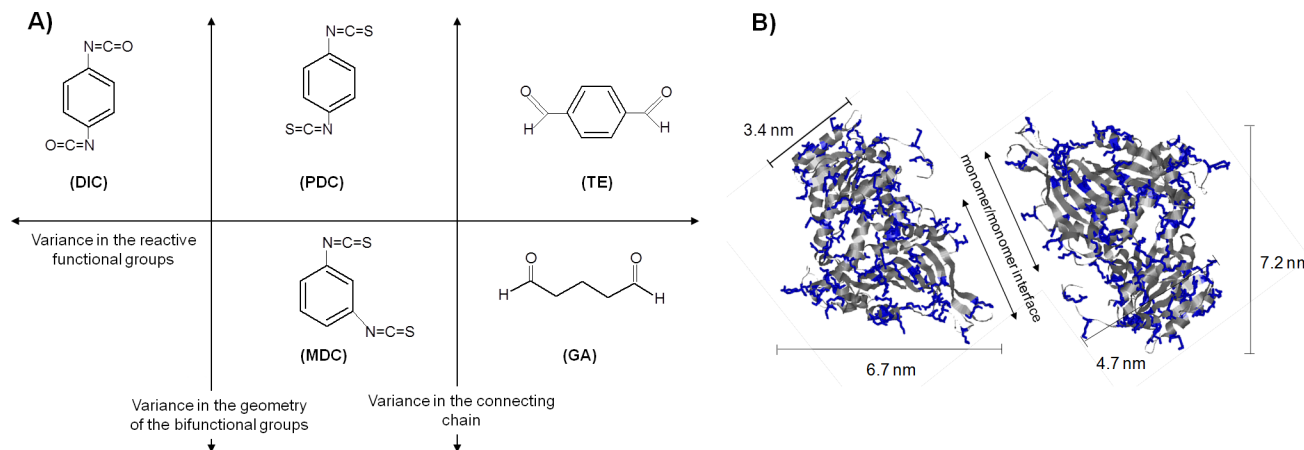


**Figure 1.** (A) Molecular structure of cross-linkers: 1,4-phenylene diisocyanate (DIC), 1,4-phenylene diisothiocyanate (PDC), 1,3-phenylene diisothiocyanate (MDC), Glutaraldehyde (GA), and Terephthalaldehyde (TE). (B) 3-D structure of G6PDH monomer (PDB, code P11412) and the distribution of the superimposed residues (Lys and Arg) from a monomer. Two views of the distribution of the amino acid residues are presented, corresponding to the two monomers. Association at the interface forms the G6PDH dimer. Figures and sizes were generated using Rasmol 2.7.5.2.

protein at the other end (via  $-\text{NH}_2$  residues of the enzyme molecules). In the event that the enzyme exhibits many  $-\text{NH}_2$  residues in its side chains, this may lead to multiple anchoring sites ("multipoints" grafting), thereby restricting the conformational changes and limiting the loss of enzyme activity. However, only a few investigations have addressed the influence of cross-linkers on the enzyme–surface interactions.<sup>10,11</sup> The surface modification procedure was originally designed with a specific chemical scenario in mind, and therefore many studies are blind to evidence that this scenario is not working as planned. Very often, the formation of covalent bonds is not demonstrated and the occurrence or improvement of enzymatic activity in the resulting systems could as well be attributed to noncovalent bonding between the enzyme and the silanized substrate.<sup>12</sup> Furthermore, in the aqueous media used for biological applications, the silane layer may be subjected to strong chemical and morphological modifications,<sup>13–15</sup> thus influencing its function as an anchoring layer. Accordingly, understanding the behavior of the immobilized enzymes requires coping with the complexity of the interfaces and the multiple physicochemical processes influencing the success of enzyme attachment.<sup>16</sup>

In this study, enzyme immobilization was performed on a silanized silicon wafer after treatment with a linker. To this end, a variety of linkers were used, differing by their reactive functional group (isocyanate:  $-\text{NCO}$ , isothiocyanate:  $-\text{NCS}$ , or aldehyde:  $-\text{CHO}$ ), by the nature of the connecting chain (aliphatic or aromatic), and by the geometry of the bifunctional groups positioned meta- or para- to the aromatic cycle as depicted in Figure 1A. Enzyme adsorption was monitored *in situ* using quartz crystal microbalance with dissipation monitoring (QCM-D), and surface characterizations were performed by X-ray photoelectron spectroscopy (XPS) and atomic force microscopy (AFM). The evolution of the interfacial phases as a function of the linker used is examined in depth and its impact on the enzymatic activity is discussed.

## 2. MATERIALS AND METHODS

**2.1. Materials.** Silicon wafers  $\langle 100 \rangle$  were cut into  $0.9 \times 0.9 \text{ cm}^2$  pieces, glucose-6-phosphate dehydrogenase from baker's yeast (G6PDH, EC 1.1.1.49,  $206 \text{ U} \cdot \text{mg}^{-1}$ ), D-glucose-6-phosphate sodium salt (G6P),  $\beta$ -nicotinamide adenine

dinucleotide phosphate ( $\text{NADP}^+$ ) hydrate,  $\beta$ -nicotinamide adenine dinucleotide phosphate reduced tetra(cyclohexylammonium) salt (NADPH),  $\text{Na}_2\text{HPO}_4$ ,  $\text{NaH}_2\text{PO}_4$ , 3-aminopropyl(triethoxysilane) (APTES, 98%), grade II glutaraldehyde (GA, 25%), terephthalaldehyde (TE, 99%), 1,4-phenylenediisocyanate (DIC), 1,4-phenylenediisothiocyanate (PDC, 98%), 1,3-phenylenediisothiocyanate (MDC, 97%),  $N,N$ -dimethylformamide (DMF,  $\geq 99\%$ ), and pyridine ( $\geq 99\%$ ) were purchased from Sigma-Aldrich (France),  $\text{H}_2\text{O}_2$  (30%) and toluene from Prolabo (VWR, France) and  $\text{H}_2\text{SO}_4$  (96%) from Carlo Erba (France). All products were used without further purification.

**2.2. Sample Preparation.** **2.2.1. Silicon Wafers Cleaning.** Prior to sample silanization, wafer surfaces were cleaned, using a sonication bath (70 W, 40 kHz, Branson, USA), first in acetone for 10 min, then in a binary mixture of acetone and ethanol (50/50, v/v) for 10 min, and rinsed abundantly with ultrapure water (Milli-Q, Millipore, France). Samples were then immersed in freshly prepared piranha solution (30%  $\text{H}_2\text{O}_2$  and 96%  $\text{H}_2\text{SO}_4$  mixed in 1:3 ratio) for 15 min. (Caution: piranha solution is a strong oxidant and reacts violently with organic substances!) These substrates were then thoroughly washed in ultrapure water and dried under nitrogen gas flow. Finally, the samples were treated during 2 h in a UV-ozone cleaner (Bioforce Nanosciences), and stored in ultrapure water before use.

**2.2.2. Surface Treatment Procedure.** Surface silanization was performed using APTES according to the protocol detailed elsewhere (high temperature protocol).<sup>13</sup> Silanized samples are called "Sil". The latter were subjected to treatments with cross-linkers using different bifunctional cross-linkers (DIC, PDC, MDC, GA, and TE) as described previously.<sup>17</sup> The surfaces after this treatment are designated as "Sil-C.L.", where "C.L." is the name of the cross-linker. The adsorption of enzymes (G6PDH,  $100 \mu\text{g} \cdot \text{mL}^{-1}$ , phosphate buffer, 50 M, pH  $\sim 7.4$ ) was then performed for 2 h either on Sil sample ("Sil-Ez") or on Sil-C.L. samples ("Sil-C.L.-Ez"). The samples were then rinsed twice with phosphate buffer and dried under nitrogen gas flow.

**2.3. Atomic Force Microscopy (AFM).** AFM images were recorded using a commercial AFM (NanoScope VIII Multi-Mode AFM, Bruker Nano Inc.- Nano Surfaces Division, Santa Barbara, CA) equipped with a  $150 \times 150 \times 5 \mu\text{m}^3$  scanner (J-

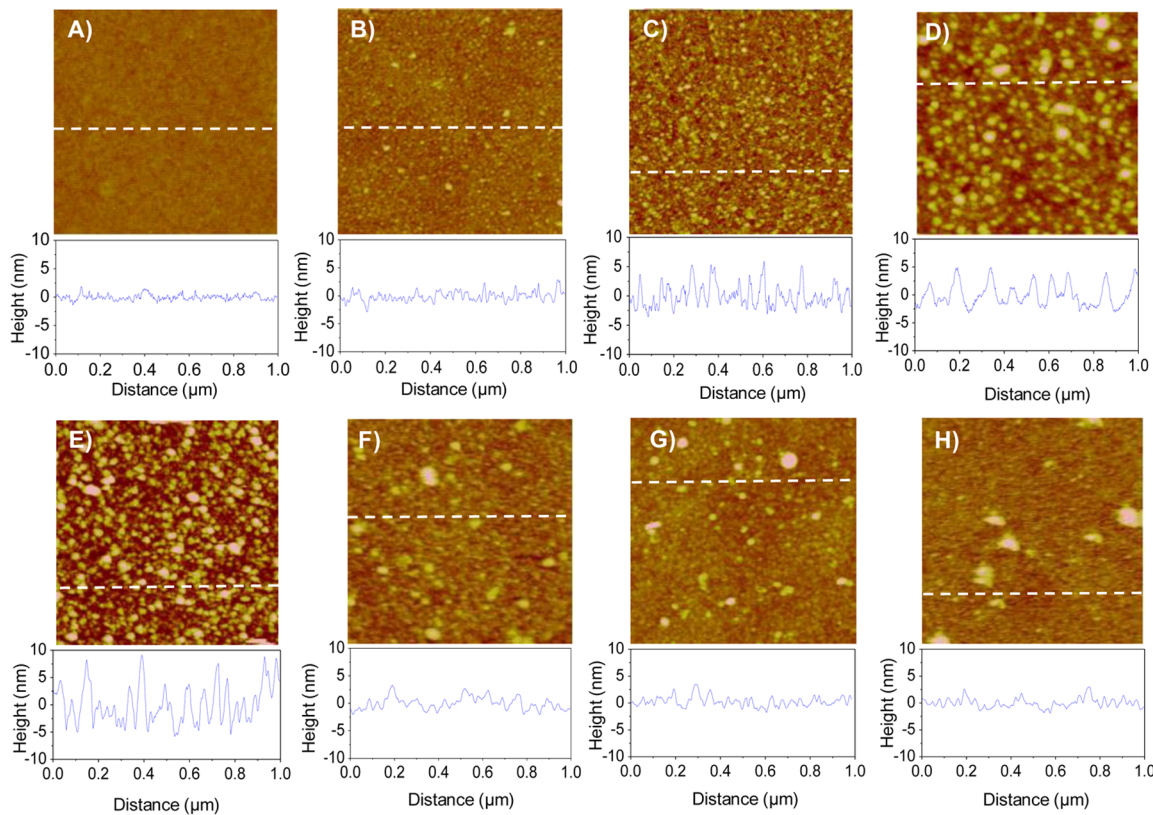


**Figure 2.** AFM height images (peak force tapping mode, in phosphate buffer; z-scale 20 nm; image size  $1 \times 1 \mu\text{m}^2$ ) recorded on (A) bare silicon oxide (Si), (B) silanized silicon oxide (Sil), (C) after enzyme adsorption without previous linker treatment, (D–H) after treatment with linker and subsequent enzyme adsorption on (D) DIC, (E) PDC, (F) MDC, (G) GA, and (H) TE. Cross sections were taken at the place indicated by the dashed line.

scanner). A quartz fluid cell was used without the O-ring. The silicon wafers were fixed on a steel sample puck using adhesive tape. The mounted samples were immediately transferred into the AFM liquid cell taking care to avoid dewetting. Images were recorded in peak force tapping mode in a buffer at room temperature ( $\sim 22\text{--}24^\circ\text{C}$ ) using oxide-sharpened micro-fabricated  $\text{Si}_3\text{N}_4$  cantilevers (Bruker Nano Inc.- Nano Surfaces Division, Santa Barbara, CA). The spring constants of the cantilevers were measured using the thermal noise method, yielding values ranging from 0.4 to 0.45 N/m. The curvature radius of silicon nitride tips was lower than 10 nm (manufacturer specifications). All images shown in this paper are flattened raw data.

**2.4. XPS Analysis.** XPS analyses were performed using a SPECS (Phoibos MCD 100), X-ray photoelectron spectrometer (SPECS, Germany) equipped with a monochromatized aluminum X-ray source ( $h\nu = 1486.74 \text{ eV}$ ), and Phoibos 100 hemispherical energy analyzer. A pass energy of 20 eV was used for survey scan and 10 eV for narrow scans. The samples were fixed on the support, and no charge stabilization device was used. The pressure in the analysis chamber during measurement was around  $10^{-10}$  Torr. The photoelectron collection angle,  $\theta$ , between the normal to the sample surface and the analyzer axis was  $0^\circ$ . The following sequence of spectra was recorded: survey spectrum, O 1s, N 1s, C 1s, Si 2p, and S 2s. The data treatment was performed with the Casa XPS software (Casa Software Ltd., UK). The peaks were decomposed using a linear baseline, and a component shape defined by the product of a Gauss and Lorentz function, in a 70:30 ratio. Molar

concentration ratios were calculated using peak areas normalized according to Scofield factors.

**2.5. Quartz Crystal Microbalance with Dissipation Monitoring (QCM-D).** Enzyme adsorption on the silicon substrate was followed *in situ* by quartz crystal microbalance with dissipation monitoring. Measurements were performed with a Q-Sense E1 system (Gothenborg, Sweden) at a temperature of  $24.0 \pm 0.1^\circ\text{C}$ . The crystal used was a thin AT-cut quartz coated with a thin  $\text{SiO}_2$  film (thickness  $\sim 50 \text{ nm}$ ) provided by Q-Sense. It was cleaned as previously described for silicon wafers. Oscillations of the crystal at the resonant frequency (5 MHz) or at one of its overtones (15, 25, 35, 45, 55, 65 MHz) were obtained when applying ac voltage. The variations of the resonance frequency ( $\Delta f$ ) and of dissipation ( $\Delta D$ ) were monitored upon adsorption of the enzyme. Solutions were injected into the measurement cell using a peristaltic pump (Ismatec IPC-N 4) at a flow rate of  $50 \mu\text{L}\cdot\text{min}^{-1}$ . Prior to enzyme adsorption, a phosphate buffer solution was injected up to signal stabilization. The protein solution was then brought into the measurement cell until the frequency and dissipation signal reached a stationary value. Subsequently, rinsing was performed using a phosphate buffer solution. All QCM-D experiments were carried out on at least two different samples for each condition.

**2.6. Enzyme Activity.** The studied enzyme is D-glucose-6-phosphate dehydrogenase (G6PDH) which catalyzes the oxidation of D-glucose-6-phosphate (G6P) yielding gluconolactone-6-phosphate and uses  $\beta$ -nicotinamide adenine dinucleotide phosphate ( $\text{NADP}^+$ ) as cofactor. The enzyme activity was evaluated by monitoring the production of NADPH

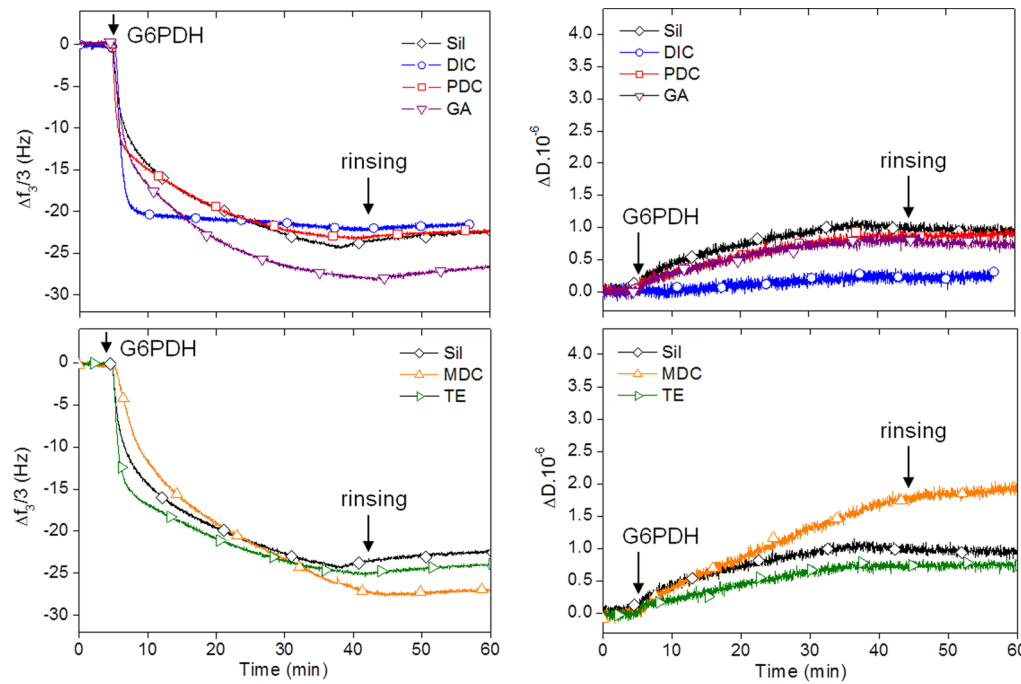


**Figure 3.** QCM-D measurements showing frequency changes in the 3<sup>rd</sup> overtone (left) and the corresponding dissipation change (right) vs time during enzyme adsorption on silanized silicon surface and using the different cross-linkers.

spectrophotometrically, following the procedure described elsewhere.<sup>17</sup>

The thermal stability of immobilized enzymes was determined by incubating the samples in a phosphate buffer (50 mM, pH ~7.4) at 30 or 40 °C for 1 h. The samples were then brought to room temperature while being kept in the buffer and the enzyme activity was determined again. The residual activities were expressed relative to the original activity assayed at room temperature.

### 3. RESULTS AND DISCUSSION

**3.1. Surface Morphology.** Surface characterization using AFM imaging is difficult to carry out on silanized surfaces, especially in the presence of adsorbed proteins. This is due to (i) the softness of biological materials, (ii) the mobility of adsorbed biomolecules at the solid/liquid interface and (iii) the possible desorption of some compounds (silanes or proteins) and their tendency to interact with the AFM tip. Significant improvements have been obtained thanks to the development of the peak force tapping mode.<sup>18,19</sup> In this AFM method, the applied force is lower than in the classical tapping mode, thus allowing probing the interface with minimal disturbance. AFM images recorded in phosphate buffer solution prior to and after the different treatments are presented in Figure 2. The bare silicon surface exhibited a relatively smooth surface ( $R_{\text{rms}} = 0.41$  nm, Figure 2A). After silanization, the roughness increased to a limited degree ( $R_{\text{rms}} = 0.84$  nm, Figure 2B), owing to the formation of a silane layer as demonstrated in our previous study.<sup>13</sup>

The adsorption of the enzyme without cross-linker (Sil-Ez sample, Figure 2C) led to the appearance of particles uniformly distributed on the surface and showing an appreciable increase of surface roughness ( $R_{\text{rms}} = 1.32$  nm, Figure 2C). Cross sections indicated that isolated particles have fairly uniform heights, around ~4 nm. They may correspond to adsorbed enzymes, taking into account the dimensions of the enzyme in a

random orientation (Figure 1B) and considering the possible conformational changes in contact with the surface. However, it is difficult to discriminate between the different multimeric forms (mono-, di-, or tetramer) in the adsorbed phase, as this would require higher lateral resolution.

When using DIC and PDC cross-linkers for enzyme immobilization, the surface morphology was radically modified as compared to the silanized surface. The cross sections indicated that the particles were not homogeneous in size; many of them were below 5 nm in height but some reached 10 nm, revealing the formation of aggregates ( $R_{\text{rms}} = 3.14$  and 1.90 nm for PDC and DIC, respectively). Interestingly, the formation of aggregates was not observed when the geometry of the spacer molecule was changed; namely, it was not present when the meta-disubstituted MDC was used instead of the para-disubstituted PDC. Dialdehyde coupling agents (GA and TE) differing by the aliphatic or aromatic nature of the spacer chains, also showed a difference in particle density and size (Figure 2G and H). The surface roughness was  $R_{\text{rms}} = 0.96$  and 0.77 nm for GA and TE, respectively. It is noteworthy that the formation of aggregates could not be attributed to the sole effect of cross-linker: in fact, as reported in previous studies, the activation of silanized surfaces with cross-linkers did not noticeably change the surface topography.<sup>20,21</sup> Accordingly, it is reasonable to conclude that the nanostructures observed with AFM correspond to the supramolecular organization of the adsorbed enzymes which seems to be greatly affected by the nature of the cross-linker used.

**3.2. QCM-D Study.** The adsorption of enzymes on silane-modified surfaces using the different linkers was monitored *in situ* by QCM-D. The frequency shift ( $\Delta f$ ) and dissipation ( $\Delta D$ ) are shown for the different samples as a function of time (Figure 3). The enzyme adsorption was observed through the shift of frequency toward negative values (between -20.65 and -25.75 Hz). The dissipation values recorded remained low (Table 1); however, possibly relevant variations are observed

**Table 1.** Results from QCM-D ( $\Delta f$ ,  $\Delta D$ ,  $\Delta m^{\text{QCM-D}}$ ) and XPS ( $\Delta m^{\text{XPS}}$ ) after Enzyme Adsorption on the Silanized Surface, and on the Same Surface Modified with Coupling Agents<sup>a</sup>

	$\Delta f$ (Hz)	$\Delta D$ ( $10^{-6}$ )	$\Delta m^{\text{QCM-D}}$ (ng/cm <sup>2</sup> )	$\Delta m^{\text{XPS}}$ (ng/cm <sup>2</sup> )
Sil	-22.5 (0.0)	0.95 (0.0)	403.9 (0.0)	225.6 (5.8)
Sil-DIC	-20.65 (1.2)	0.24 (0.0)	369.9 (28.4)	436.9 (19.2)
Sil-PDC	-23.25 (1.06)	0.76 (0.18)	417.5 (25.0)	405.7 (15.0)
Sil-MDC	-25.75 (1.76)	1.96 (0.05)	452.6 (40.8)	178.1 (5.36)
Sil-GA	-25.34 (1.89)	0.83 (0.08)	456.7 (33.6)	399.9 (16.1)
Sil-TE	-24.5 (0.70)	0.67 (0.09)	445.0 (21.0)	273.6 (9.7)

<sup>a</sup>All values are given as the mean of 2 runs. Numbers between brackets indicate standard variations.

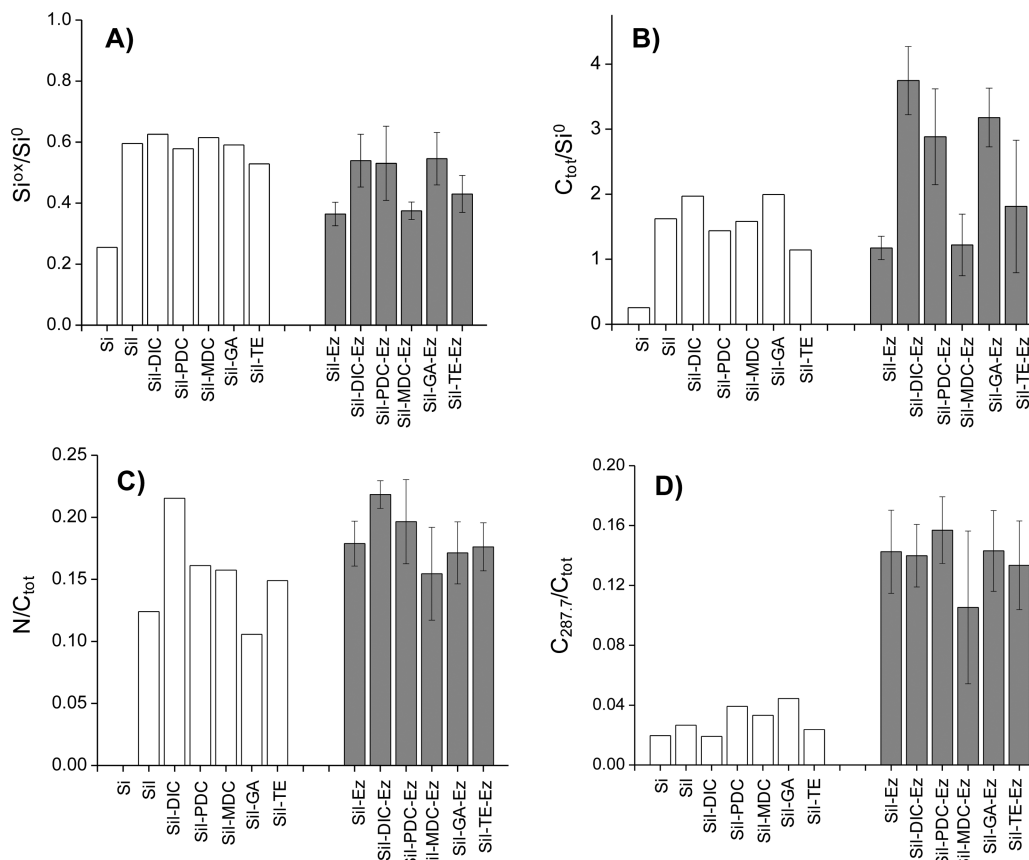


**Figure 4.** Molar concentration ratios (A)  $\text{Si}^{\text{ox}}/\text{Si}^0$ , (B)  $C_{\text{tot}}/\text{Si}^0$ , (C)  $N/C_{\text{tot}}$ , and (D)  $C_{287.7}/C_{\text{tot}}$  measured by XPS (data from Table S1, Supporting Information) on bare silicon wafer (Si), silanized surface (Sil), and silanized surfaces modified with coupling agents, prior to (white histograms: Sil-DIC, Sil-PDC, Sil-MDC, Sil-GA, and Sil-TE) and after adsorption of enzyme (gray histograms: Sil-Ez, Sil-DIC-Ez, Sil-PDC-Ez, Sil-MDC-Ez, Sil-GA-Ez, and Sil-TE-Ez). Standard deviations are an average of two independent sets of samples.

between the samples ( $\Delta D$  reached  $2.10^{-6}$  with the MDC linker and did not exceed  $1.10^{-6}$  with the other samples). The lowest dissipation value was obtained with the DIC linker at  $\sim 0.2 \times 10^{-6}$ , which is close to the detection limit (manufacturer's specifications).

QCM-D data also provide direct information regarding the adsorption kinetics of enzymes on the different surfaces through the  $\Delta f$  vs time graphs (Figure 3). It is clear that the use of DIC linker greatly accelerates the adsorption process, compared to the other samples. Moreover, on the latter samples the evolution of the frequency shifts revealed the presence of two kinetically different steps (Figure 3). The first step is rapid, as it takes about 2.5 min (Figure 3). It could be attributed to the first establishment of an interaction between the enzymes and the surface. The second step is by contrast much slower and may be attributed to interfacial processes

related to the rearrangement of the adsorbed phase, including conformational changes, supramolecular organization, changes in the degree of hydration,<sup>22,23</sup> etc. Even though similar behavior has been reported for the adsorption of several other proteins,<sup>24,25</sup> these conclusions must be considered with caution, owing to potential problems with the stability of the underlying silane layer (see discussion in section 3.4).

The frequency shifts recorded when steady state is reached may allow the amount of adsorbed enzymes to be evaluated when applying the appropriate model and considering certain assumptions. In the present study, the Sauerbrey relationship  $\Delta m = -C \cdot \Delta f_n / n$  was used to calculate the change in mass, where  $\Delta m$  represents the mass surface density ( $\text{ng cm}^{-2}$ ),  $C$  is a proportionality constant that depends only on the intrinsic properties of the sensor ( $C = 17.7 \text{ ng cm}^{-2} \text{ Hz}^{1/2}$  for AT-cut quartz sensor),  $\Delta f_n$  is the frequency shift, and  $n$  is the overtone

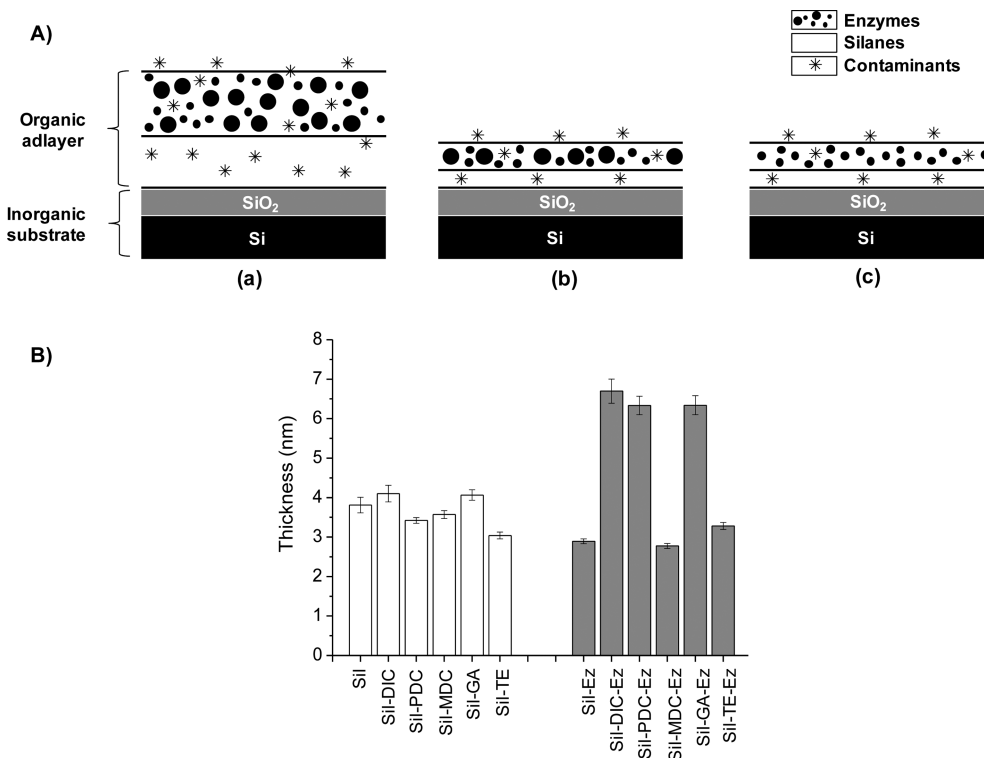


**Figure 5.** Panel (A): Schematic representation of the wafer surface after silanization and enzyme immobilization. Illustration of the evolution of interfacial phases upon enzyme immobilization when the silane layer remains stable (a), or is subjected to significant degradation (b, c). Organic contaminants are denoted with stars. Panel (B): Average thickness values of the organic adlayer ( $t_{\text{org}}$ ) deduced from XPS measurements on silanized silicon wafer, as such and modified with linkers, before (white) and after enzyme adsorption (gray).

number. The use of the Sauerbrey model is justified if the adsorbed layer is rigid and laterally homogeneous. The independence of the frequency shift on the overtone number (Supporting Information, Figure S1) is, indeed, a strong argument in favor of this model. Furthermore, according to some authors, the Sauerbrey model can be reasonably considered when the  $(\Delta D_n)/(\Delta f_n/n)$  ratio is lower than  $0.4 \times 10^{-6}$ .<sup>26</sup> Using the Sauerbrey relation, results showed that  $\Delta m^{\text{QCM-D}}$  values are in the same range when the enzymes are adsorbed on the different surfaces, except for DIC which showed a significantly lower  $\Delta m^{\text{QCM-D}}$  value (Table 1).

**3.3. XPS Analysis.** **3.3.1. Evolution of the Organic Adlayer.** Figure 4 provides a practical way to evaluate the chemical composition of the treated silicon surfaces. Figure 4A presents the  $\text{Si}^{\text{ox}}/\text{Si}^0$  molar concentration ratios of the different samples (data from Table S1), which illustrate the evolution of the silicon in the Si oxide with respect to the nonoxidized silicon substrate ( $\text{Si}^0$ ). Upon silanization, this ratio increased markedly to reach values around 0.6 (compare Si and Sil samples, Figure 4A), indicating successful surface silanization. When silanized samples are treated with the linkers, no noticeable evolution of the  $\text{Si}^{\text{ox}}/\text{Si}^0$  ratio can be observed which is indicative of the silane layer stability under treatments with linkers (Figure 4A). The same trend, i.e., unchanging  $\text{Si}^{\text{ox}}/\text{Si}^0$  molar ratio, was also observed after the subsequent adsorption of enzymes when using DIC, PDC, and GA linkers. In contrast, a significant decrease of  $\text{Si}^{\text{ox}}/\text{Si}^0$  ratio was noticed when using MDC and TE or without linker. These observations can be explained either by a degradation of the silane layer or by a dissolution of the silicon oxide. The latter hypothesis, even though it has been documented on silicon wafers after incubation in a variety of biological fluids,<sup>14</sup> can be

ruled out in the present study since the solubility of silicon oxide is at a minimum level at pH values ranging from 7 to 8 and only increases at higher pH.<sup>27</sup> Furthermore, the effect of incubation of bare and silanized silicon wafers in a phosphate buffer (pH = 7.2) has been investigated in a recent paper, showing no significant influence on the native oxide layer, when the surface is silanized.<sup>14</sup> Therefore, degradation of the silane layer is probably the most likely explanation in the these two instances.

The evolution of the amount of organic compounds can be evaluated from the variation of total carbon ( $C_{\text{tot}}$ ) with respect to the nonoxidized silicon substrate ( $\text{Si}^0$ ), since we can assume that the thickness of the  $\text{SiO}_2$  layer does not change significantly. Prior to silanization, the presence of adventitious contamination, mainly of hydrocarbon nature (see C 1s peak, Figure S2, Supporting Information), is observed, but its amount is rather low, compared to other high surface energy solids.<sup>16,28,29</sup> The  $C_{\text{tot}}/\text{Si}^0$  molar ratio increased markedly after silanization; however, only little variation can be observed after a further treatment with linkers, regardless of the molecule used (Figure 4B), suggesting that the composition of the silane layer was not subjected to noticeable change. In contrast, after the adsorption of enzymes, the  $C_{\text{tot}}/\text{Si}^0$  ratio increased markedly when using DIC, PDC, or GA linkers (Figure 4B) which may indicate the presence of immobilized enzymes on the surface in significant amounts. The situation with the other two linkers, i.e., MDC and TE, and when the adsorption was performed without any linker (Figure 4B) was different as the  $C_{\text{tot}}/\text{Si}^0$  ratio remained almost unchanged or even decreased slightly. This evolution of  $C_{\text{tot}}/\text{Si}^0$  cannot be correlated to the amount of adsorbed enzymes in a direct way, because other

compounds, mainly silanes and contaminants, are contributing to the total carbon molar concentration ( $C_{\text{tot}}$ ).

These remarks are qualitative. A quantitative evaluation of the adlayer thickness may clarify whether the variation of  $\text{Si}^{\text{ox}}$  and  $C_{\text{tot}}$  concentration with respect to the nonoxidized silicon substrate ( $\text{Si}^0$ ), resulting from the different treatments, reflects an addition of or a substitution by new compounds in the adlayer. The thickness of the organic adlayer can be evaluated by XPS if we consider the model, described in Figure 5A, involving the silicon substrate with an oxide layer, the silane layer, and an enzyme layer. This model does not take into account a layer of contamination but supposes instead that contaminants are equally distributed within the organic adlayer (contaminants are represented as stars in Figure 5A). The silicon oxide layer thickness ( $t_{\text{SiO}_2}$ ) can be evaluated using eq 1 in Supporting Information. The  $t_{\text{SiO}_2}$  value obtained on nonsilanized samples was 1.5 nm, in agreement with previous studies using a similar surface preparation procedure.<sup>14,15</sup>

In a similar way, the thickness of the organic adlayer ( $t_{\text{org}}$ ) can be evaluated from the  $C_{\text{tot}}/\text{Si}^0$  molar concentration ratios, using eq 2 (Supporting Information). Figure 5B presents the average values of the organic adlayer thickness, computed for the different samples prior to (white bars) and after enzyme adsorption (gray bars). The thickness of the organic adlayer,  $t_{\text{org}}$ , after surface silanization and further treatment with linkers was almost the same, independently of the linker used. After enzyme immobilization, the thickness of the organic adlayer increased markedly on silanized sample treated with DIC, PDC, and GA linkers. By contrast, when enzymes were adsorbed without linker or by using MDC or TE, the thickness remained almost unchanged or decreased slightly (Figure 5B). In previous studies using a similar silanization procedure, the thickness of the silane layer was evaluated at about 2.3 nm.<sup>30,31</sup> In the present study,  $t_{\text{org}}$  values include a contribution of adventitious contamination with an average contribution to the thickness of about 1 nm.<sup>15</sup> Accordingly,  $t_{\text{org}}$  values reported in Figure 5 are close to those reported in refs 30 and 31.

**3.3.2. Chemical Speciation of the Organic Adlayer.** The evolution of the nature of adsorbed organic compounds as a function of the different treatments was examined by following the  $\text{N}/C_{\text{tot}}$  molar ratio, commonly used as a tool to reveal a surface enrichment with proteins (on biomaterials,<sup>32</sup> cell surfaces,<sup>33,34</sup> etc.). Figure 4C shows that the evolution of  $\text{N}/C_{\text{tot}}$  does not reveal any clear trend as a function of the treatment. This is due to (i) the significant variation of  $C_{\text{tot}}$  as evidenced by the  $C_{\text{tot}}/\text{Si}^0$  (Figure 4B), and (ii) the fact that the nitrogen peak includes contributions originating from both the silane end groups and proteins. By contrast, the  $\text{C}_{287.7}$  component (mostly corresponding to carbonyl groups) may be used as a marker of protein compounds. The evolution of  $\text{C}_{287.7}/C_{\text{tot}}$  evidenced, indeed, a noticeable increase after enzyme adsorption (compare white and gray histograms in Figure 4D). This result confirms the enrichment of the organic adlayer with enzymes, independently of the linker used, in agreement with QCM-D measurements.

The trends in surface composition appear more clearly if they are summarized in terms of concentration of model molecular compounds. The compounds taken into account in the present system are silanes (Sil), proteins (Pr), and contaminants which are mainly hydrocarbon-like compounds (HC). The chemical composition and density considered for these model compounds are listed in Table S2 (Supporting Information).

The proportion of carbon atoms due to each model compound X ( $C_X/C_{\text{tot}}$ ) can be computed by solving the system of eqs 3, 4, 5, detailed in the Supporting Information.

The experimental concentration ratios ( $C_X/C_{\text{tot}}$ ) can be converted into weight percentages of model compounds,<sup>35,36</sup> using the chemical concentration specific to each compound (Table S2). Results given in Table 2 show that the amount of

**Table 2. Chemical Composition (Weight %) of the Organic Adlayer Present on Silanized Surfaces, and on the Same Surfaces Modified with Coupling Agents, as Deduced from XPS Data and Expressed in Terms of Classes of Molecular Compounds<sup>a</sup>**

	(wt %)		
	Sil	Prot	HC
Sil	79.9	(7.6)	12.4
Sil-DIC	76.2	(5.8)	18.0
Sil-PDC	81.8	(10.7)	7.5
Sil-MDC	82.6	(9.1)	8.3
Sil-GA	69.6	(13.8)	16.5
Sil-TE	85.6	(6.4)	8.0
Sil-Ez	41.0	48.4	10.6
Sil-DIC-Ez	35.6	50.1	14.2
Sil-PDC-Ez	41.2	52.3	6.5
Sil-MDC-Ez	47.7	36.1	16.2
Sil-GA-Ez	41.0	48.8	10.2
Sil-TE-Ez	46.1	44.4	9.5

<sup>a</sup>Data between brackets are protein equivalent of adventitious contamination and have no physical meaning.

(hydrocarbon-like) contaminants remains low compared to the other constituents, independently of the surface treatment. Prior to the adsorption of enzymes, the samples exhibited the predominant presence of silanes. The concentration of proteins on these samples (data between brackets in Table 2) is non-negligible but variable, and may be attributed to adventitious contamination. After adsorption of enzymes, a drastic increase of protein concentration with respect to silane was observed for all samples, whether a linker is used or not (Table 2), suggesting an enrichment of the organic adlayer with protein compounds.

**3.4. State of the Interface.** The adsorption of enzymes was confirmed on all treated samples by *in situ* QCM-D measurements and *ex situ* XPS analysis, as described above. On the silanized surface without linker, the adsorption may occur through hydrophobic interaction (water contact angle on silanized surface  $\sim 65^\circ$ ) or more probably via electrostatic attraction between the protonated terminal groups of the grafted silanes and the negatively charged enzyme (enzyme isoelectric point = 5.9; adsorption performed at pH 7.4). By using cross-linkers, the mechanism of attachment, if it involves covalent bonds, is expected to occur according to a random multipoint attachment, as described elsewhere.<sup>17,37,38</sup> This is due to the distribution over all the enzyme surface (Figure 1B) of the  $-\text{NH}_2$  residues able to interact with the functional groups of the linkers. Covalent attachment is difficult to demonstrate from XPS analysis because the formation of an amide bond could not be discriminated against peptidic links present in a high amount in the attached enzyme (see the evolution of  $\text{C}_{287.7}/C_{\text{tot}}$  Figure 4D). It was shown that the immobilization of enzymes via DIC, PDC, or GA linkers

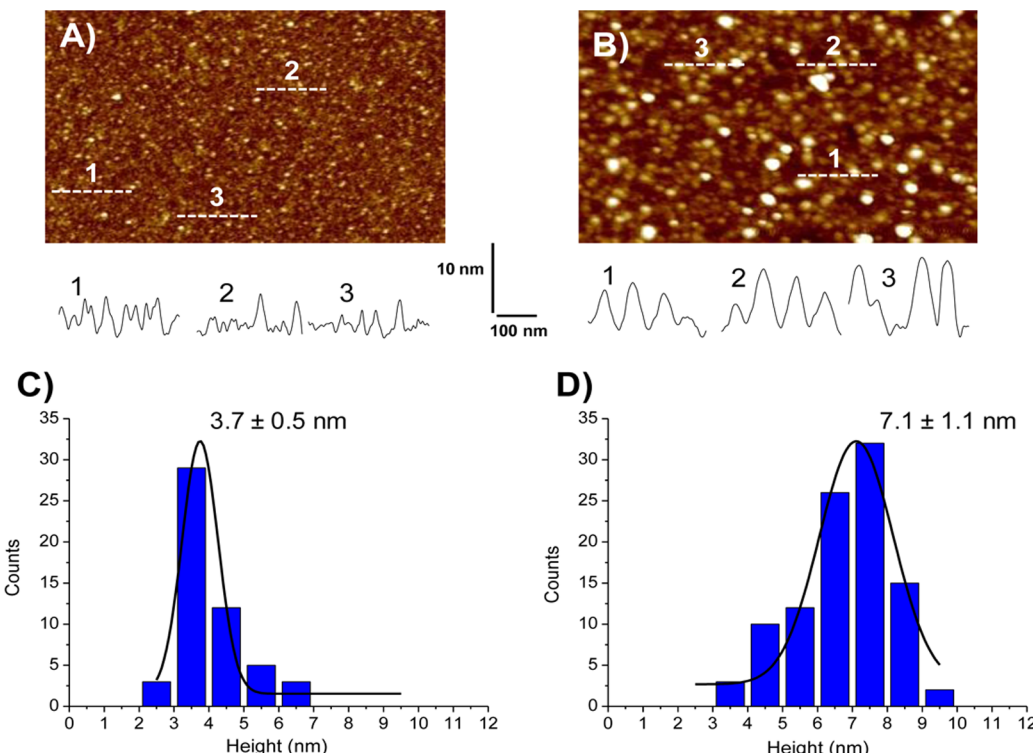


**Figure 6.** (A, B) AFM height images (peak force tapping mode, in phosphate buffer; z-scale 20 nm) of silanized silicon oxide (A) after enzyme adsorption without previous linker treatment and (B) after treatment with DIC and subsequent enzyme adsorption. Cross sections were taken at the different locations indicated by the dashed line and numbered. (C, D) Histograms of the aggregate heights corresponding to images (A) and (B), respectively.

consists of the addition of an enzyme layer on the silane anchoring layer, the latter remaining stable during the adsorption process. This result is supported by the evolutions of  $\text{Si}^{\text{ox}}/\text{Si}^0$  and  $C_{\text{tot}}/\text{Si}^0$  ratios (Figure 4A,B), on one hand, and  $t_{\text{org}}$  (Figure 5B), on the other hand, which are compatible with an addition of enzymes onto the silanized surfaces when using DIC, PDC, and GA linkers. In these cases, the alteration of the silane layer is not significant. By contrast, when enzyme adsorption was carried out on a silanized sample without a linker, or treated with MDC and TE, the interfacial processes were radically modified. Enzyme adsorption induced a degradation of the silane layer, as unambiguously evidenced by the decrease of the  $\text{Si}^{\text{ox}}/\text{Si}^0$  molar ratio (Figure 4A). This degradation was only partial, as the  $\text{Si}^{\text{ox}}/\text{Si}^0$  value remained significantly higher than that for nonsilanized sample (Figure 4A). In our previous study, this evolution of the silane layer upon adsorption of proteins (without linker) was not detected by using IR analysis (GA-ATR mode), because the method used to quantify IR data, based on the measurement of band intensities, provides only semiquantitative information and is not able to detect small variations. In contrast, noticeable silane degradation was evidenced using the same method when silanization was performed at room temperature.<sup>13</sup> The use of XPS analysis is more appropriate in this context, as the technique is very sensitive to evidence and quantify weak variations when investigating the composition of thin solid films.

The mechanism by which the silane layer degrades in aqueous media with biological interest may be related to the hydrophobic character of the layer. Indeed, the presence of a hydrophobic film may prevent the penetration of water into the  $\text{SiO}_2/\text{silane}$  interface, thus stabilizing the silane layer.<sup>39–41</sup>

Water contact angle measurements performed on silanized samples after further treatment with linkers revealed noticeably higher values for DIC, PDC, and GA ( $60^\circ$ ,  $71^\circ$ , and  $56^\circ$ , respectively) compared to MDC and TE ( $49^\circ$  and  $44^\circ$ , respectively). These results are compatible with the correlation between the hydrophobic character and the stability of the silane layer. Accordingly, DIC, PDC, and GA linkers play a major role in preserving silane from dissolution upon enzyme adsorption. Therefore, it was possible to discuss adsorption kinetics for these three samples (see section 3.2). By contrast, when silane degradation occurs upon enzyme adsorption, the latter phenomenon makes the QCM-D signal difficult to interpret, particularly in terms of adsorption kinetics. Comparison can, however, be made between DIC, PDC, and GA, revealing that the former linker allowed adsorption to be performed most rapidly.

The AFM images show that the organization of the adsorbed enzymes depends on the linker, revealing significant variations in the level of aggregation (Figure 2). This makes the estimation of the adsorbed amount of enzymes by means of QCM-D or XPS a challenging task. The mass obtained by QCM-D,  $\Delta m^{\text{QCM-D}}$ , corresponds to a “wet” mass, owing to the contribution of coupled water molecules which may be entrapped within the layer, but the amount of coupled water is influenced by the state of aggregation of adsorbed proteins at the interface.<sup>42,43</sup> Furthermore, the formation of aggregates at the interface may bring additional complexity to the exploration of QCM-D data which is essentially related to hydrodynamic considerations.<sup>43–46</sup>

XPS may also provide an estimate of the adsorbed proteins, which corresponds to a “dry” mass ( $\Delta m^{\text{XPS}}$ ). This can be given by:  $\Delta m^{\text{XPS}} = t_{\text{org}} \times \rho \times \text{wt}_{\text{prot}}(\%)$ , where  $\rho$  is the density of the

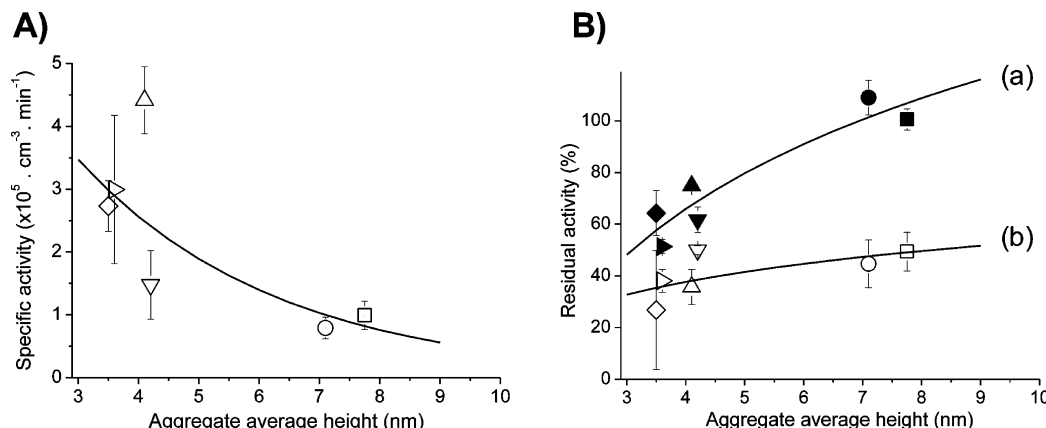


**Figure 7.** (A) Specific activity as a function of the aggregate average heights, as determined with AFM, of immobilized enzymes on silanized silicon surface (Sil,  $\diamond$ ) and using the different cross-linkers: (DIC,  $\circ$ ), (PDC,  $\square$ ), (MDC,  $\triangle$ ), (GA,  $\nabla$ ), and (TE,  $\triangleright$ ). (B) Thermal stability of immobilized enzymes on the same samples as a function of the aggregate average heights. Samples were incubated in a phosphate buffer for 1 h at (a) 30 °C (closed symbols) and (b) 40 °C (open symbols). The percentage is relative to the original activity assayed without heating. Error bars correspond to the standard deviations of three independent experiments. The black curves are optical guidelines.

enzyme ( $1.4 \text{ g.cm}^{-3}$ ) and  $\text{wt}_{\text{prot}}(\%)$  is the weight percentage of proteins (data from Table 2). The results in Table 1 show noticeable variations as a function of the linker used. Particularly, the amounts of adsorbed proteins on silanized surface without linker or when using MDC or TE linkers were significantly lower than when using DIC, PDC, and GA. Even though the calculation of  $t_{\text{org}}$  can be influenced by the variation of the surface roughness, the trend observed with ( $\Delta m^{\text{XPS}}$ ) was not affected by the use of either a model of continuous adlayer (see Figure 5) or a discontinuous adlayer, taking into account the degree of surface coverage (data not shown). It must be kept in mind that sample drying and its further storage under vacuum may influence the state of the interface. These phenomena remain poorly understood.<sup>12</sup>

In summary, the evolution of the interfacial phases upon enzyme immobilization as a function of the linker used may be described according to the scheme depicted in Figure 5A. Situation (a) corresponds to the interface obtained when using DIC, PDC, or GA linkers, while situation (b) describes the evolution of interfacial phases with MDC or TE, where enzyme adsorption induces a significant degradation of the silane layer and results on the immobilization of lower enzyme amounts. Situation (c), relative to the silanized surface without a linker, is similar to situation (b). However, we must keep in mind that between situations (b) and (c), while similarly low values are observed for  $t_{\text{org}}$  (Figure 5B) and  $\Delta m^{\text{XPS}}$  (Table 1), the main differences concern the enzyme layer morphology, as revealed by AFM, showing well dispersed particles on the silanized sample (Figure 2C) and a few randomly dispersed aggregates when MDC or TE are used as linkers (Figure 2F and H). The variation of the adlayer thickness ( $t_{\text{org}}$ ) is thus due to (i) the partial degradation of the silane layer and (ii) the difference of morphology, as evidenced by AFM images (Figure 2), resulting from the supramolecular organization of immobilized enzymes.

**3.5. Enzyme Activity.** The variation of the catalytic activity of the enzyme as a function of the linker used was detailed in a previous study.<sup>17</sup> The operational and thermal stability of the immobilized enzymes were investigated in depth, showing large differences between the procedures using different cross-linking molecules. These effects may be described on the basis of the multipoint attachment model, in which the three-dimensional structure, including the quaternary structure, is supposed to be

stabilized when the number of anchoring points is high.<sup>17,37</sup> In the present study, the enzyme activity is examined as a function of the supramolecular organization of molecules at the interface. Indeed, AFM images revealed that cross-linkers strongly influence the organization of immobilized enzymes, showing noticeable disparities in the level of aggregation (Figure 2). The average size of the aggregates was determined on the basis of AFM images, as shown in Figure 6. A height size distribution was estimated on the basis of several cross sections performed along  $1 \times 1 \mu\text{m}^2$  images. As a case in point, typical cross sections obtained on immobilized enzymes on silanized sample without linker (Figure 6A) or by using DIC as linker (Figure 6B) showed significant differences in average heights. In the former case, enzymes were well dispersed and the average height observed could correspond to the size of a single enzyme (see Figure 1B), although the discrimination between the different multimeric forms remains difficult, as mentioned above. By contrast, when using DIC, the formation of aggregates was obvious with an average height around 7 nm (Figure 6D).

The evolution of enzyme activity as a function of the average height of the aggregates is given in Figure 7. Specific activities were deduced from the quantification of immobilized enzymes obtained with XPS (data from Table 1). The results showed that the specific activity decreased markedly when the aggregate size increased (Figure 7A). The lowest values were obtained when using DIC and PDC linkers, while MDC and TE showed specific activity almost as high as that obtained without a linker (Figure 7A). This disadvantageous effect of aggregation is, indeed, expected and may be associated with diffusional constraints.<sup>47</sup>

The activity of the studied enzyme is particularly sensitive to heating owing to its multimeric structure. In aqueous solutions, the enzyme is predominantly in tetrameric and dimeric forms, but only the latter form is catalytically active. Based on DSC (differential scanning calorimetry) measurements, it has been shown that dissociation of the dimer into monomers occurs at a temperature around 50 °C, leading to irreversible enzyme inactivation.<sup>17</sup> In the present study, the effect of the level of aggregation on the thermostability of immobilized enzymes was investigated at temperatures lower than the one at which dimer dissociation occurs. After heating at 40 °C, a loss of activity was

observed for all samples, regardless of the linker used (Figure 7B). The situation was however different after 30 °C heating. The residual activity was around 50% for silanized sample, but it increased markedly when the size of aggregate increased (Figure 7B). Particularly, when DIC or PDC were used as linkers the activity was almost totally preserved.

This trend provides a clear picture regarding the performance of the studied systems. Interestingly, it allows the establishment of a structure–function relationship, correlating the effect of the supramolecular organization, i.e., the formation of aggregates, to the preservation of enzymatic activity. It appears that aggregates may enhance the stability of the tridimensional structure of proteins as observed elsewhere, including at the single-molecule level.<sup>48,49</sup> In our study, the compactness of the structure, through enzyme aggregation, may influence the tertiary structure, by promoting intramolecular stabilizing forces of the monomer<sup>50</sup> and stabilizing the native state by sterically hindering conformational change,<sup>48</sup> but also the quaternary structure by the assembly of the different subunits, and probably the stability of the active dimeric form by hydrophobic interactions at the monomer–monomer interface.

#### 4. CONCLUSION

The immobilization of G6PDH was performed on a silanized surface by means of short cross-linking molecules. The different steps of surface treatment were characterized by XPS analysis, and enzyme adsorption and organization were monitored by *in situ* QCM-D measurements and by AFM. A detailed examination of XPS data provided an identification of the adsorbed compounds and an evaluation of their amount. The thickness of the organic adlayer was computed and its elemental composition was converted into concentrations of model organic compounds: silanes, enzymes, and contaminants. We observed that the silane layer is sensitive to the linker used and may undergo significant degradation upon enzyme adsorption. By using DIC, PDC, or GA linkers, no silane degradation was observed and enzymes were adsorbed in significant amounts, leading to the formation of a dense packing of aggregates (specifically with DIC and PDC linkers). On the contrary, when MDC was used instead of PDC (linker groups positioned in meta- and para- of the aromatic cycle, respectively), interfacial processes were strongly modified: the silane layer was partly degraded and the amount of adsorbed enzymes was markedly reduced. The two aldehyde linkers, GA and TE, which differ by the nature of their connecting chains (aliphatic or aromatic, respectively), also showed noticeable differences both in the silane layer stability and in the amount of immobilized enzymes.

On the silanized surface without a linker, the amount of immobilized enzymes was as low as in the case of MDC and TE linkers, and a degradation of the silane layer was observed for these three samples. These results clearly show that the cross-linker has an effect on both silane layer stability and the amount of immobilized enzyme. The QCM-D study also shows that the use of linkers did not seriously affect the mechanism of adsorption, except in the case of DIC for which enzyme adsorption occurred more rapidly.

The variation of the state of aggregation greatly influenced the enzyme activity. A structure–function relationship was thus established, showing that the activity decreased when the size of enzyme aggregates increased. By contrast, increasing the size of the aggregates significantly improved the thermostability of the immobilized enzyme.

The present study points out the relevance of correlating the organization of an interface with biological interest to the bioactivity of adsorbed molecules. It also provides practical information and allows the immobilization of enzymes to be carried out under optimized conditions. Furthermore, the approach used can be extended to other macromolecules with biological interest, including peptides and DNA, and is relevant for applications such as antifouling, biosensing, and cell culture.

#### ■ ASSOCIATED CONTENT

##### S Supporting Information

QCD monitoring, XPS analysis, surface concentration data, thickness and concentration calculations, and chemical composition. This material is available free of charge via the Internet at <http://pubs.acs.org>.

#### ■ AUTHOR INFORMATION

##### Corresponding Author

\*E-mail address: jessem.landoulsi@upmc.fr.

##### Notes

The authors declare no competing financial interest.

#### ■ ACKNOWLEDGMENTS

N.A. acknowledges the financial support of the AUF (Agence Universitaire de la Francophonie).

#### ■ REFERENCES

- (1) Kim, J.-H.; Choi, D.-C.; Yeon, K.-M.; Kim, S.-R.; Lee, C.-H. Enzyme-Immobilized Nanofiltration Membrane To Mitigate Biofouling Based on Quorum Quenching. *Environ. Sci. Technol.* **2011**, *45*, 1601–1607.
- (2) Betancor, L.; Johnson, G. R.; Luckarift, H. R. Stabilized Laccases as Heterogeneous Bioelectrocatalysts. *ChemCatChem* **2013**, *5*, 46–60.
- (3) Akoh, C. C.; Chang, S.-W.; Lee, G.-C.; Shaw, J.-F. Biocatalysis for the Production of Industrial Products and Functional Foods from Rice and Other Agricultural Produce. *J. Agric. Food Chem.* **2008**, *56*, 10445–10451.
- (4) Talbert, J. N.; Goddard, J. M. Enzymes on Material Surfaces. *Colloids Surf., B* **2012**, *93*, 8–19.
- (5) Subramanian, A.; Kennel, S. J.; Oden, P. I.; Jacobson, K. B.; Woodward, J.; Doktycz, M. J. Comparison of Techniques for Enzyme Immobilization on Silicon Supports. *Enzyme Microb. Technol.* **1999**, *24*, 26–34.
- (6) Sarah Babu, V. R.; Kumar, M. A.; Karanth, N. G.; Thakur, M. S. Stabilization of Immobilized Glucose Oxidase against Thermal Inactivation by Silanization for Biosensor Applications. *Biosens. Bioelectron.* **2004**, *19*, 1337–1341.
- (7) Hähl, H.; Evers, F.; Grandthyll, S.; Paulus, M.; Sternemann, C.; Loskill, P.; Lessel, M.; Hüsecken, A. K.; Brenner, T.; Tolan, M.; Jacobs, K. Subsurface Influence on the Structure of Protein Adsorbates as Revealed by *In Situ* X-ray Reflectivity. *Langmuir* **2012**, *28*, 7747–7756.
- (8) Rusmini, F.; Zhong, Z.; Feijen, J. Protein Immobilization Strategies for Protein Biochips. *Biomacromolecules* **2007**, *8*, 1775–1789.
- (9) Jonkheijm, P.; Weinrich, D.; Schröder, H.; Niemeyer, C. M.; Waldmann, H. Chemical Strategies for Generating Protein Biochips. *Angew. Chem., Int. Ed.* **2008**, *47*, 9618–9647.
- (10) Tiller, J. C.; Rieseler, R.; Berlin, P.; Klemm, D. Stabilization of Activity of Oxidoreductases by Their Immobilization onto Special Functionalized Glass and Novel Aminocellulose Film Using Different Coupling Reagents. *Biomacromolecules* **2002**, *3*, 1021–1029.
- (11) Vallières, K.; Chevallier, P.; Sarra-Bourret, C.; Turgeon, S.; Laroche, G. AFM Imaging of Immobilized Fibronectin: Does the Surface Conjugation Scheme Affect the Protein Orientation/Conformation? *Langmuir* **2007**, *23*, 9745–9751.

- (12) Landoulsi, J.; Genet, M. J.; Kirat, K. E.; Richard, C.; Pulvin, S.; Rouxhet, P. G. Silanization with APTES for Controlling the Interactions Between Stainless Steel and Biocomponents: Reality vs Expectation. In *Biomaterials - Physics and Chemistry*, Pignatello, R., Ed.; Intech Publisher (online), 2011; pp 99–126.
- (13) Aissaoui, N.; Bergaoui, L.; Landoulsi, J.; Lambert, J.-F.; Boujday, S. Silane Layers on Silicon Surfaces: Mechanism of Interaction, Stability, and Influence on Protein Adsorption. *Langmuir* **2012**, *28*, 656–665.
- (14) Dekeyser, C. M.; Buron, C. C.; Derclaye, S. R.; Jonas, A. M.; Marchand-Brynaert, J.; Rouxhet, P. G. Degradation of Bare and Silanized Silicon Wafer Surfaces by Constituents of Biological Fluids. *J. Colloid Sci.* **2012**, *378*, 77–82.
- (15) Dekeyser, C. M.; Buron, C. C.; Mc Evoy, K.; Dupont-Gillain, C. C.; Marchand-Brynaert, J.; Jonas, A. M.; Rouxhet, P. G. Oligo(ethylene glycol) Monolayers by Silanization of Silicon Wafers: Real Nature and Stability. *J. Colloid Sci.* **2008**, *324*, 118–126.
- (16) Caillou, S.; Gerin, P. A.; Nonckreman, C. I. J.; Fleith, S.; Dupont-Gillain, C. C.; Landoulsi, J.; Pancera, S. M.; Genet, M. J.; Rouxhet, P. G. Enzymes at Solid Surfaces: Nature of the Interfaces and Physico-Chemical Processes. *Electrochim. Acta* **2008**, *54*, 116–122.
- (17) Aissaoui, N.; Landoulsi, J.; Bergaoui, L.; Boujday, S.; Lambert, J.-F. Catalytic Activity and Thermostability of Enzymes Immobilized on Silanized Surface: Influence of the Crosslinking Agent. *Enzyme Microb. Technol.* **2013**, *52*, 336–343.
- (18) Adamcik, J.; Berquand, A.; Mezzenga, R. Single-Step Direct Measurement of Amyloid Fibrils Stiffness by Peak Force Quantitative Nanomechanical Atomic Force Microscopy. *Appl. Phys. Lett.* **2011**, *98*, 193701–3.
- (19) Landoulsi, J.; Dupres, V. Direct AFM Force Mapping of Surface Nanoscale Organization and Protein Adsorption on Aluminum Substrate. *Phys. Chem. Chem. Phys.* **2013**, *15*, 8429–8440.
- (20) Blasi, L.; Longo, L.; Vasapollo, G.; Cingolani, R.; Rinaldi, R.; Rizzello, T.; Acierno, R.; Maffia, M. Characterization of Glutamate Dehydrogenase Immobilization on Silica Surface by Atomic Force Microscopy and Kinetic Analyses. *Enzyme Microb. Technol.* **2005**, *36*, 818–823.
- (21) Saal, K.; Sammelselg, V.; Lohmus, A.; Kuusk, E.; Raidaru, G.; Rinken, T.; Rinken, A. Characterization of Glucose Oxidase Immobilization onto Mica Carrier by Atomic Force Microscopy and Kinetic Studies. *Biomol. Eng.* **2002**, *19*, 195–199.
- (22) Paul, S.; Paul, D.; Basova, T.; Ray, A. K. Studies of Adsorption and Viscoelastic Properties of Proteins onto Liquid Crystal Phthalocyanine Surface Using Quartz Crystal Microbalance with Dissipation Technique. *J. Phys. Chem. C* **2008**, *112*, 11822–11830.
- (23) Wang, X.; Liu, G.; Zhang, G. Effect of Surface Wettability on Ion-Specific Protein Adsorption. *Langmuir* **2012**, *28*, 14642–14653.
- (24) Borges, J.; Campina, J. M.; Souza, H. K. S.; Goncalves, M. P.; Silva, A. F. Aggregation-Induced Conformational Transitions in Bovine  $\beta$ -Lactoglobulin Adsorbed onto Open Chitosan Structures. *Soft Matter* **2012**, *8*, 1190–1201.
- (25) Molino, P. J.; Higgins, M. J.; Innis, P. C.; Kapsa, R. M. I.; Wallace, G. G. Fibronectin and Bovine Serum Albumin Adsorption and Conformational Dynamics on Inherently Conducting Polymers: A QCM-D Study. *Langmuir* **2012**, *28*, 8433–8445.
- (26) Reviakine, I.; Johannsmann, D.; Richter, R. P. Hearing What You Cannot See and Visualizing What You Hear: Interpreting Quartz Crystal Microbalance Data from Solvated Interfaces. *Anal. Chem.* **2011**, *83*, 8838–8848.
- (27) Wasserman, S. R.; Tao, Y. T.; Whitesides, G. M. Structure and Reactivity of Alkylsiloxane Monolayers Formed by Reaction of Alkyltrichlorosilanes on Silicon Substrates. *Langmuir* **1989**, *5*, 1074–1087.
- (28) Landoulsi, J.; Genet, M. J.; Richard, C.; El Kirat, K.; Pulvin, S.; Rouxhet, P. G. Evolution of the Passive Film and Organic Constituents at the Surface of Stainless Steel Immersed in Fresh Water. *J. Colloid Interface Sci.* **2008**, *318*, 278–289.
- (29) Mantel, M.; Rabinovich, Y. I.; Wightman, J. P.; Yoon, R. H. A Study of Hydrophobic Interactions between Stainless Steel and Silanated Glass Surface Using Atomic Force Microscopy. *J. Colloid Interface Sci.* **1995**, *170*, 203–214.
- (30) Zhu, M.; Lerum, M. Z.; Chen, W. How To Prepare Reproducible, Homogeneous, and Hydrolytically Stable Aminosilane-Derived Layers on Silica. *Langmuir* **2011**, *28*, 416–423.
- (31) Howarter, J. A.; Youngblood, J. P. Optimization of Silica Silanization by 3-Aminopropyltriethoxysilane. *Langmuir* **2006**, *22*, 11142–11147.
- (32) Zoulalian, V.; Zürcher, S.; Tosatti, S.; Textor, M.; Monge, S.; Robin, J.-J. Self-Assembly of Poly(ethylene glycol)-Poly(alkyl phosphonate) Terpolymers on Titanium Oxide Surfaces: Synthesis, Interface Characterization, Investigation of Nonfouling Properties, and Long-Term Stability. *Langmuir* **2009**, *26*, 74–82.
- (33) Ahimou, F.; Boonaert, C. J. P.; Adriaensen, Y.; Jacques, P.; Thonart, P.; Paquot, M.; Rouxhet, P. G. XPS Analysis of Chemical Functions at the Surface of *Bacillus subtilis*. *J. Colloid Interface Sci.* **2007**, *309*, 49–55.
- (34) Dufrene, Y. F.; Rouxhet, P. G. Surface Composition, Surface Properties, And Adhesiveness of *Azospirillum Brasilense*-Variation during Growth. *Can. J. Microbiol.* **1996**, *42*, 548–556.
- (35) Genet, M. J.; Dupont-Gillain, C. C.; Rouxhet, P. G. XPS Analysis of Biosystems and Biomaterials. In *Medical Applications of Colloids*, Matijevic, E., Ed.; Springer: New York, 2008.
- (36) Rouxhet, P. G.; Genet, M. J. XPS Analysis of Bio-Organic Systems. *Surf. Interface Anal.* **2012**, *43*, 1453–1470.
- (37) Fernandez-Lafuente, R. Stabilization of Multimeric Enzymes: Strategies to Prevent Subunit Dissociation. *Enzyme Microb. Technol.* **2009**, *45*, 405–418.
- (38) Rodrigues, R. C.; Ortiz, C.; Berenguer-Murcia, A.; Torres, R.; Fernandez-Lafuente, R. Modifying Enzyme Activity and Selectivity by Immobilization. *Chem. Soc. Rev.* **2013**, *42*, 6290–6307.
- (39) Wang, A.; Cao, T.; Tang, H.; Liang, X.; Salley, S. O.; Ng, K. Y. S. In Vitro Haemocompatibility and Stability of Two Types of Heparin-Immobilized Silicon Surfaces. *Colloids Surf., B* **2005**, *43*, 245–255.
- (40) Pegg, E. C.; Walker, G. S.; Scotchford, C. A.; Farrar, D.; Grant, D. Mono-Functional Aminosilanes As Primers for Peptide Functionalization. *J. Biomed. Mater. Res., Part A* **2009**, *90A*, 947–958.
- (41) Tsukagoshi, T.; Kondo, Y.; Yoshino, N. Protein Adsorption and Stability of Poly(Ethylene Oxide)-Modified Surfaces Having Hydrophobic Layer between Substrate and Polymer. *Colloids Surf., B* **2007**, *54*, 82–87.
- (42) Carton, I.; Brisson, A. R.; Richter, R. P. Label-Free Detection of Clustering of Membrane-Bound Proteins. *Anal. Chem.* **2010**, *82*, 9275–9281.
- (43) Rojas, E.; Gallego, M.; Reviakine, I. Effect of Sample Heterogeneity on the Interpretation of Quartz Crystal Microbalance Data: Impurity Effects. *Anal. Chem.* **2008**, *80*, 8982–8990.
- (44) Johannsmann, D.; Reviakine, I.; Richter, R. P. Dissipation in Films of Adsorbed Nanospheres Studied by Quartz Crystal Microbalance (QCM). *Anal. Chem.* **2009**, *81*, 8167–8176.
- (45) Johannsmann, D.; Reviakine, I.; Rojas, E.; Gallego, M. Effect of Sample Heterogeneity on the Interpretation of QCM(-D) Data: Comparison of Combined Quartz Crystal Microbalance/Atomic Force Microscopy Measurements with Finite Element Method Modeling. *Anal. Chem.* **2008**, *80*, 8891–8899.
- (46) Urbakh, M.; Daikhin, L. Influence of the Surface Morphology on the Quartz Crystal Microbalance Response in a Fluid. *Langmuir* **1994**, *10*, 2836–2841.
- (47) Hirsh, S. L.; Bilek, M. M. M.; Nosworthy, N. J.; Kondyurin, A.; dos Remedios, C. G.; McKenzie, D. R. A Comparison of Covalent Immobilization and Physical Adsorption of a Cellulase Enzyme Mixture. *Langmuir* **2010**, *26*, 14380–14388.
- (48) Gouda, M. D.; Singh, S. A.; Rao, A. G. A.; Thakur, M. S.; Karanth, N. G. Thermal Inactivation of Glucose Oxidase. Mechanism and Stabilization Using Additives. *J. Biol. Chem.* **2003**, *278*, 24324–33.
- (49) Meadows, P. Y.; Bemis, J. E.; Walker, G. C. Single-Molecule Force Spectroscopy of Isolated and Aggregated Fibronectin Proteins on Negatively Charged Surfaces in Aqueous Liquids. *Langmuir* **2003**, *19*, 9566–9572.

(50) Anand, G.; Sharma, S.; Dutta, A. K.; Kumar, S. K.; Belfort, G. Conformational Transitions of Adsorbed Proteins on Surfaces of Varying Polarity. *Langmuir* **2010**, *26*, 10803–10811.